COMPOSITE MICRO-SCALE MODEL ACCOUNTING FOR DEBONDING, STRAIN RATE-DEPENDENCE AND DAMAGE UNDER IMPACT USING AN EXPLICIT FINITE ELEMENT SOLVER

F.A. Gilabert[1,2], D. Garoz[1,2], R.D.B. Sevenois[1,2], S.W.F. Spronk[1,2], A. Rezaei[1,2], W. Van Paepegem[1]

[1] Department of Materials Science and Engineering, Faculty of Engineering and Architecture,
Ghent University. Tech Lane Ghent Science Park – Campus A,
Technologiepark-Zwijnaarde 903, B-9052 Zwijnaarde (Ghent), Belgium.
Email: fran.gilabert@ugent.be, Web Page: http://www.composites.ugent.be
[2]SIM vzw, M3 program, Technologiepark-Zwijnaarde 935, B-9052 Zwijnaarde (Ghent), Belgium.

Keywords: Composites, Micro-scale modeling, Strain-rate effects, Damage, Explicit solver

Abstract

This work presents a micro-scale simulation model that can be used to analyze the mechanical response of unidirectional fiber reinforced composite materials undergoing high strain rates. A periodic Representative Volume Element (RVE) composed of randomly spaced fibers embedded in a polymer matrix is used. The model can include features like fiber-matrix debonding, strain-rate dependency and matrix failure. The material model is based on the kinematic formulation where the deformation gradient is decomposed into elastic and inelastic parts. The strain-rate dependency is incorporated via a physically based flow rule of the inelastic part of the deformation gradient. As an application of the proposed model, a RVE that represents a carbon/epoxy system undergoing a transversal tensile load is used. The implementation of the periodic boundary conditions makes it possible to distinguish fibers and matrix as well as the Poisson's effects. Fibers are transversely isotropic and linear elastic. The flow rule that governs the strain-rate dependency of the epoxy matrix is identified via lab tests using pure matrix specimens under tension. The resulting homogenized stress-strain curves are obtained and linked to the micro-mechanical features. The influence of the strain-rate effect on the stress distribution and damage pattern is discussed.

1. Introduction

Industrial sectors like aeronautics, marine or wind energy are leading the use of composites. All of them are nowadays introducing a multiscale approach in their cycles of design, because the complexity of composites is high and different levels of description are necessary to introduce details of their internal architecture and material features. A multiscale treatment is composed of several linked descriptions. In this work, three levels are distinguished: microscale, mesoscale and macroscale. The understanding of the internal mechanisms of composites (for example, fiber debonding at microscale level, or ply delamination at mesoscale level), is required to improve features like higher energy absorption capabilities under impact or crack growth control under fatigue. This work is focused on the microscale level, where the three basic components of a composite are represented: fibers, matrix and fiber-matrix interface. This allows us to see how and when degradation processes occur at different deformation rates with sufficient detailed. An adequate material design is the key point to establish which phenomena are truly relevant in order to capture the behavior of the composite material. The present model gathers simultaneously strain-rate dependency, debonding and fracture. The results of the present microscopic description can be fed into the mesoscopic level (either to represent the behavior of a yarn or to represent an entire UD

ply).

2. Formulation in brief

This model is developed using an explicit finite element solver and it relies on the combination of two modeling components: (i) the material model is implemented by means of a user subroutine written in C++ programming language, and (ii) the interface between fibers and matrix is implemented using a built-in general contact formulation endowed with a cohesive traction-separation interaction law.

The material model is based on the kinematic formulation where the total deformation gradient is multiplicatively decomposed into elastic and inelastic parts [1] as follows

$$\boldsymbol{F} = \boldsymbol{F}_e\boldsymbol{F}_i \tag{1}$$

where letters "e" and "i" stand for elastic and inelastic, respectively. In the present model, the material experiences inelastic deformations and therefore only the elastic deformation gradient $\boldsymbol{F}_e$ is used to obtain the Cauchy elastic stress tensor, given by

$$\sigma_e = \frac{1}{\det[\boldsymbol{F}_e]}\Big(\lambda\,\mathrm{tr}[\boldsymbol{h}]\,\boldsymbol{I} + 2\mu\,\boldsymbol{h}\Big) \tag{2}$$

where λ and μ are the Lamé parameters, $\boldsymbol{I}$ is the identity tensor, $\boldsymbol{h} = \log\left(\sqrt{\boldsymbol{B}_e}\right)$ is the Hencky strain tensor that accounts for large deformations in a purely elastic material and $\boldsymbol{B}_e = \boldsymbol{F}_e\boldsymbol{F}_e^T$ is the elastic Cauchy-Green tensor.

The strain-rate dependency is incorporated via a physically based flow rule during the integration over time of the inelastic part of the deformation gradient. For an isotropic material, the rate of deformation gradient change can be expressed as $\dot{\boldsymbol{F}}_i = \boldsymbol{D}_i\boldsymbol{F}_i$ (for more details, see [2, 3]). $\boldsymbol{D}_i$ represents the inelastic rate of deformation and it can be used to insert the constitutive relationships to include strain-rate dependency of the strength, elasticity and degradation features. The inelastic rate of deformation is linked to the constitutive model of strain-rate dependency by $\boldsymbol{D}_i = \dot{\epsilon}\boldsymbol{N}$, where $\boldsymbol{N}$ is the direction tensor and $\dot{\epsilon}$ contains the prescribed flow rule. This work focuses on the strain-rate dependency of the strength of the polymer matrix via a visco-plastic model. To that aim, several constitutive models are available to represent this inelastic deformation in glassy polymer. Most of them are based on the theoretical approach proposed by Argon [4], who studied the thermally-activated mechanism of yielding in glassy polymers. This theory has been successfully applied to describe a wide variety of amorphous polymers like epoxy, PMMA, PC or PS, among others [5–10]. The basic constitutive model is given by

$$\dot{\epsilon} = \dot{\epsilon}_0 \exp\Big[-\frac{A}{K_BT}s\Big(1-\Big(\frac{\tau}{s}\Big)^{5/6}\Big)\Big] \tag{3}$$

where $\dot{\epsilon}_0$ is a pre-exponential factor related to the production of pairs of molecular kinks in the unit volume [4, 11], A is the activation energy, K_B is the Boltzmann constant, τ is the shear stress, s represents a micro-scale athermal shear strength and T is the absolute temperature.

3. Polymer matrix material

The flow rule that governs the strain-rate dependency of the epoxy matrix has been identified via preliminary lab tests using pure matrix specimens under tension. For this initial identification, no damage features of the real tests have been used. Although a more complete study to explore different strain rates is in progress, the flow rule used in this work can be preliminary identified with the combination of experimental tests under quasi-static conditions and data obtained by other authors for epoxy resins at

F.A. Gilabert, D. Garoz, R.D.B. Sevenois, S.W.F. Spronk, A. Rezaei and W. Van Paepegem
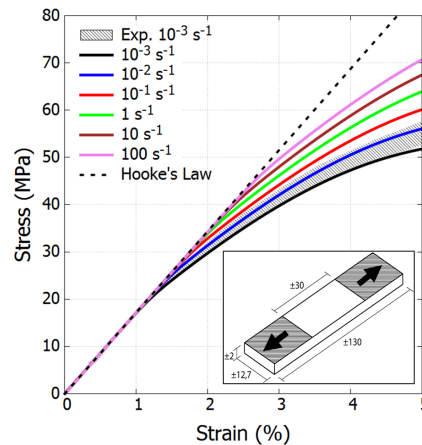
Figure 1. Stress-strain curves of pure matrix specimens under tension. Shaded pattern: experimental quasi-static results. Lines: model prediction at different strain rates. Inset: specimen dimensions, in mm.

different strain rates [8, 10, 12]. Figure 1 shows the stress-strain curves obtained from a simulation setup using the same specimen dimension and conditions as in the experiment. These specimens consisted of rectangular coupons subjected to simple tension, whose dimensions are indicated in the inset of Fig. 1. The shaded pattern in these curves represents the experimental results of a set of six coupons tested with a strain rate equal to 10^{-3} s^{-1}. The continuous lines correspond to the prediction of the simulation model at different strain rates. More details about the process of the identification of parameters can be consulted in refs. [7, 13].

The Young's modulus of the matrix from the test was 1720 MPa. The matrix Poisson's coefficient was set equal to 0.38, which is common for epoxy resins [14]. As a first approach, the two basic rate-dependent sensitivity constants of the flow rule (see Eq. 3) were obtained from ref. [12], whose values are A/K_B = 155 K/MPa and $\dot{\epsilon}_0$ = $1.9 \cdot 10^5$ s^{-1}. Figure 1 shows that this set of values can represent the pure epoxy resin used in this work. As mentioned before, additional validation under different strain rates is currently in progress.

4. Fibers and fiber-matrix interface

The reinforcing elements used in the present micro-mechanical model of composite are linear elastic and transversely isotropic carbon fibers. The interaction that connects these embedded fibers in the polymer matrix has been described through a surface-based cohesive behavior. This behavior follows a classical traction-separation law built using bi-linear cohesive zone model [15]. This interaction feature is incorporated in a built-in general contact formulation available in the finite element package used for this work. This description makes it possible to describe full contact, under compression, tension and shear, between fibers and the surrounding matrix. More details of this contact formulation can be seen in [16]. Regarding the properties, both the elastic coefficients of the fibers and the properties of the fiber-matrix interface have been obtained from ref. [17].

5. Strain-rate and damage coupling

Regarding the coupling between the strain-rate and matrix failure, the model described in section 2 is enriched with an additional module based on isotropic continuous damage mechanics. This coupling is integrated in the same user subroutine used to implement the model summarized in section 2. During the

F.A. Gilabert, D. Garoz, R.D.B. Sevenois, S.W.F. Spronk, A. Rezaei and W. Van Paepegem

workflow of this model, it is assumed that the matrix material fails when the elastic strain energy per unit volume stored in the element exceeds the amount G/l_{elem}, where G is the fracture energy (unit: J/m^2) and l_{elem} stands for the characteristic element length (unit: m).
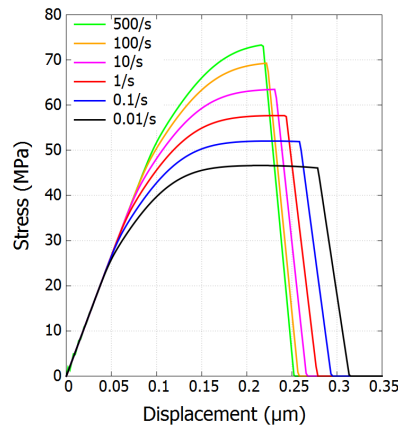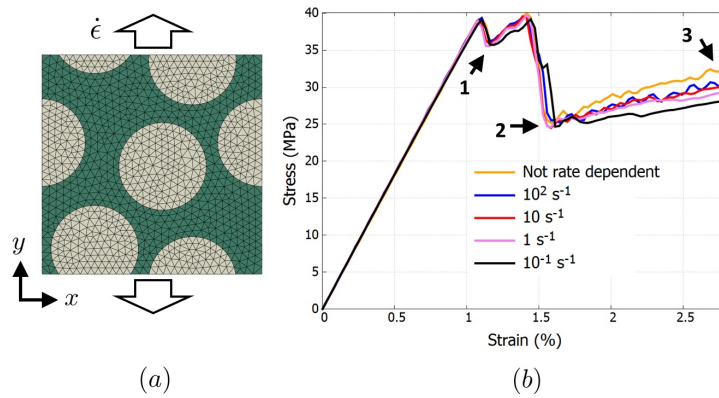

Figure 2. Example of stress-displacement curves of the rate-dependent model coupled with damage.

Figure 2 shows an example of the coupled response of the matrix model performed on single cubic element with a size of 3 μm. As it can be seen, the model of epoxy resin of Fig. 1 predicts an increase of the peak stress as the deformation rate increases. This behavior agrees with experimental observations (see for example [18]). Moreover, this feature occurs both under tension and compression [8]. It is also observed that under quasi-static tensile loading, the fracture can take place at a deformation level that clearly surpasses the peak of stress [12, 18]. As a consequence, this material can exhibit a considerable amount of deformation. Conversely, under very fast loading rates, the stress-strain curves practically retains a linear elastic response with a narrow non-linear region that contains the peak stress. Taking these global features into account, the main idea of this model is to include the interaction between two possible modes of degradation found in thermoset resins: (i) degradation via plastic instability, or shear yielding, described by the flow rule, and (ii) brittle fracture due to unstable crack growth, described by a decay produced by the softening stage of cohesive zone models. It is worth mentioning that, despite including these features, a clear identification of which mode has taken place during the test is not always possible in practice, because premature failure often occurs due to the presence of small imperfections or lack of homogeneity in the sample.

6. Results

Figure 3a shows the RVE used to test and analyze the material features described in previous sections. This configuration consists of a square periodic domain of 17.5 μm where 4 fibers with diameter of 7 μm are randomly embedded. The volume fraction of this RVE is approximately 50%. This value is still lower than that in UD composites (70% or higher), although it is sufficient for the purposes of this work. The periodic boundary cell undergoes a transversal and tensile load with a prescribed strain rate $\dot{\epsilon}$, and the lateral contraction due to Poisson's effects is allowed. More information about the implementation of the PBC can be consulted in another work of the present conference [19].

Figure 3b presents the homogenized stress-strain curves obtained from the model subjected to four different strain-rates, $\dot{\epsilon}$=0.1, 1, 10 and 100 s^{-1}. The homogenized stress component corresponds to the

F.A. Gilabert, D. Garoz, R.D.B. Sevenois, S.W.F. Spronk, A. Rezaei and W. Van Paepegem

(a)   (b)

Figure 3. (a) Periodic RVE model composed of 4 randomly spaced fibers in a strain-rate dependent matrix. (b) Homogenized stress-strain curve for different rates.

transversal direction, and it is calculated as

$$\sigma_{\mathrm{y}} = \frac{1}{V} \sum_{i}^{N} \hat{y} \cdot \boldsymbol{\sigma}^{(i)} \cdot \hat{y} \, \Delta V^{(i)} \qquad (4)$$

where $\boldsymbol{\sigma}^{(i)}$ and $\Delta V^{(i)}$ stand for the stress tensor and the volume carried by the i-th finite element, respectively, V is the sample volume, $\hat{y}$ is the unitary vector along the y-axis and N is the number of finite elements constituting the model. The strain is calculated by tracking the dimension change along the y-axis. The material features included in this example are debonding and strain rate dependence, without damage. The response of a pure linear elastic rate independent matrix under $\dot{\epsilon}$=100s^{-1} is also included (orange curve).

As it can be seen, all cases behave in a linear elastic way up to 1% of transversal strain. After this value, the debonding of fibers is initiated, and as a consequence, a clear drop of the homogenized stress is detected. The strain-rate dependency shows its effect when the transversal strain reaches a value of 1.5%, approximately. It can be seen that a lower deformation rate makes the matrix more compliant after debonding (black curve, for $\dot{\epsilon}$=0.1 s^{-1}). This response is consistent with the behavior of the pure epoxy resin shown in Fig. 1. It is worth mentioning that the epoxy matrix used in this work is more elastic than usual epoxy resins [20]. This might explain the relatively higher level of elastic deformation before failure. In order to visualize this response in more detail, three points labeled as **1**, **2** and **3** have been indicated. Figure 4 shows the profile of maximum principal stresses generated at these three stages. Furthermore, two cases are compared: the elastic rate independent matrix and the rate dependent one, both subjected to 100s^{-1}. The first drop indicated by point **1** is caused by the debonding of the most centered fiber. This drop is followed by a second and larger drop indicated by point **2**, in which the remaining fibers also debond from the matrix. In terms of stresses, both cases show a similar distribution in points **1** and **2**. Conversely, the last state labeled **3** indicates a clear difference of stress level, mostly caused by the strain-rate effect. As expected, the rate independent sample generates higher stresses.

Figure 5a shows the crack pattern generated by the RVE model under 0.1 s^{-1} when the damage is coupled to the strain-rate dependency. As it can be seen, two cracks that connect fibers are located in those points in which the principal stresses concentrate more efficiently. This feature is exhibited in the homogenized response as a new stress drop that prevents the RVE from resisting the applied load. In connection with experimental observations, Fig. 5b show the microscopical details obtained by Hobbiebrunken et al., when a carbon-fiber UD ply is transversely loaded [21]. Hobbiebrunken found that the debonding is

F.A. Gilabert, D. Garoz, R.D.B. Sevenois, S.W.F. Spronk, A. Rezaei and W. Van Paepegem
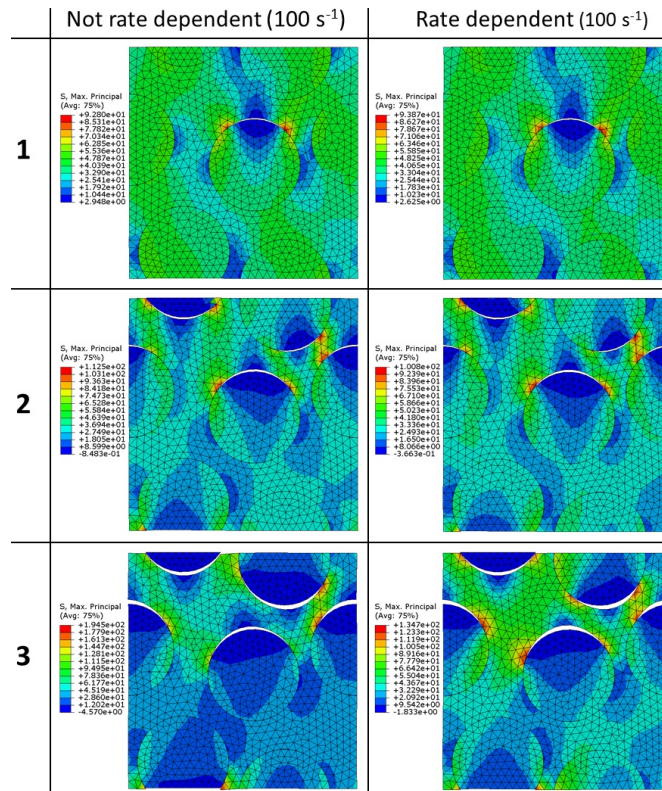
Figure 4. Profile of maximum principal stress in points **1**, **2** and **3** of Fig. 3b. (Stress in MPa).
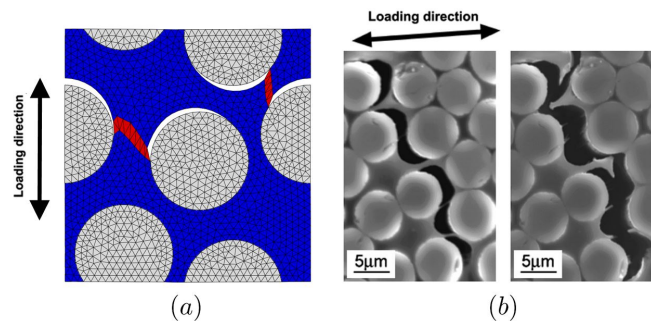
Figure 5. (a) Fracture pattern (blue=intact, red=damaged) obtained from the model when strain-rate is coupled with damage. (b) In-situ damage observations by Hobbiebrunken et al. in a carbon-fiber UD ply transversely loaded [21].

the dominating failure mechanism and multiple fibers debonded simultaneously. Moreover, as the load increases, large plastic deformation can take place in the zones of the matrix that bridge debonded fibers. The final fracture of the sample is produced when the resin bridges definitively fail. These experimental observations suggest that the proposal of the present model points to the right direction.

7. Conclusion

A simulation model designed to analyze at the micro-level unidirectional fiber reinforced composite materials is presented. The model includes three important features simultaneously that affect the macro-

F.A. Gilabert, D. Garoz, R.D.B. Sevenois, S.W.F. Spronk, A. Rezaei and W. Van Paepegem

scopic strength: fiber-matrix debonding, strain-rate dependency and failure. The strain-rate dependency is formulated using a physically based flow rule and its response under low strain rates has been compared with experimental tests. Further comparison under higher deformation rates is under progress. Damage of the material can be coupled to the strain-rate dependency. As a preliminary application of the model, a Representative Volume Element of a carbon/epoxy system is transversely loaded in tension. The homogenized mechanical response has been presented and sequence of degradation processes discussed. Similarly to in-situ experimental observations performed by other authors, the model suggests that the interfacial fiber-matrix is the dominating failure mechanism, and fiber debonding occurs simultaneously over multiple fibers. Additionally, the model accounts for plastic deformation that takes place in the zones of the matrix that bridge debonded fibers.

Acknowledgments

References

[1] E. H. Lee. Elastic-plastic deformation at finite strains. *Journal of Applied Mechanics*, 36(1):1–6, 1969.

[2] Mary C. Boyce, David M. Parks, and Ali S. Argon. Large inelastic deformation of glassy polymers. part I: rate dependent constitutive model. *Mechanics of Materials*, 7(1):15–33, 1988.

[3] M. C. Boyce, G. G. Weber, and D. M. Parks. On the kinematics of finite strain plasticity. *Journal of the Mechanics and Physics of Solids*, 37(5):647–665, 1989.

[4] A. S. Argon. A theory for the low-temperature plastic deformation of glassy polymers. *Philosophical Magazine*, 28(4):839–865, 1973.

[5] Mary C. Boyce, Ellen M. Arruda, and R. Jayachandran. The large strain compression, tension, and simple shear of polycarbonate. *Polymer Engineering & Science*, 34(9):716–725, 1994.

[6] Ellen M. Arruda, Mary C. Boyce, and R. Jayachandran. Effects of strain rate, temperature and thermomechanical coupling on the finite strain deformation of glassy polymers. *Mechanics of Materials*, 19(2–3):193–212, 1995.

[7] A.D. Mulliken and M.C. Boyce. Mechanics of the rate-dependent elasticplastic deformation of glassy polymers from low to high strain rates. *International Journal of Solids and Structures*, 43(5):1331–1356, 2006.

[8] Jennifer L. Jordan, Jason R. Foley, and Clive R. Siviour. Mechanical properties of Epon 826/DEA epoxy. *Mechanics of Time-Dependent Materials*, 12(3):249–272, 2008.

[9] K.A. Chowdhury, A.A. Benzerga, and R. Talreja. An analysis of impact-induced deformation and fracture modes in amorphous glassy polymers. *Engineering Fracture Mechanics*, 75(11):3328–3342, 2008.

[10] A. A. Benzerga, X. Poulain, K. A. Chowdhury, and R. Talreja. Computational methodology for modeling fracture in fiber-reinforced polymer composites. *Journal of Aerospace Engineering*, 22(3):296–303, 2009.

F.A. Gilabert, D. Garoz, R.D.B. Sevenois, S.W.F. Spronk, A. Rezaei and W. Van Paepegem

[11] O. A. Hasan and M. C. Boyce. A constitutive model for the nonlinear viscoelastic viscoplastic behavior of glassy polymers. *Polymer Engineering & Science*, 35(4):331–344, 1995.

[12] X. Poulain, A.A. Benzerga, and R.K. Goldberg. Finite-strain elasto-viscoplastic behavior of an epoxy resin: Experiments and modeling in the glassy regime. *International Journal of Plasticity*, 62:138–161, November 2014.

[13] M. C. Boyce and E. M. Arruda. An experimental and analytical investigation of the large strain compressive and tensile response of glassy polymers. *Polymer Engineering & Science*, 30(20):1288–1298, 1990.

[14] Stefano Pandini and Alessandro Pegoretti. Time, temperature, and strain effects on viscoelastic Poisson's ratio of epoxy resins. *Polymer Engineering & Science*, 48(7):1434–1441, 2008.

[15] K. Park and G.H. Paulino. Cohesive zone models: A critical review of traction-separation relationships across fracture surfaces. *ASME Applied Mechanics Review*, 64(6):060802/1–20, 2013.

[16] ABAQUS 6.14 User Documentation. Technical report, Dassault Systémes Simulia Corp., Providence, RI, USA., 2014.

[17] A. Arteiro, G. Catalanotti, A.R. Melro, P. Linde, and P.P. Camanho. Micro-mechanical analysis of the in situ effect in polymer composite laminates. *Composite Structures*, 116:827–840, 2014.

[18] C. Paul Buckley, J. Harding, J. P. Hou, C. Ruiz, and A. Trojanowski. Deformation of thermosetting resins at impact rates of strain. Part I: Experimental study. *Journal of the Mechanics and Physics of Solids*, 49(7):1517–1538, 2001.

[19] D. Garoz, F. A. Gilabert, R. D. B. Sevenois, S. W. F. Spronk, A. Rezaei, and W. Van Paepegem. Definition of periodic boundary conditions in explicit dynamic simulations of micro- or meso-scale unit cells with conformal and non-conformal meshes. In *17th European Conference on Composite Materials (ECCM 17)*, 2016.

[20] A. Smith, S. J. Wilkinson, and W. N. Reynolds. The elastic constants of some epoxy resins. *Journal of Materials Science*, 9(4):547–550, 1974.

[21] Thomas Hobbiebrunken, Masaki Hojo, Taiji Adachi, Claas De Jong, and Bodo Fiedler. Evaluation of interfacial strength in CF/epoxies using FEM and in-situ experiments. *Composites Part A: Applied Science and Manufacturing*, 37(12):2248–2256, December 2006.

F.A. Gilabert, D. Garoz, R.D.B. Sevenois, S.W.F. Spronk, A. Rezaei and W. Van Paepegem